Organic & Biomolecular Chemistry

ROYAL SOCIETY OF CHEMISTRY

PAPER

View Article Online
View Journal | View Issue

Cite this: *Org. Biomol. Chem.*, 2020, **18**, 7677

Synthesis and properties of chiral fluorescent helicene-BODIPY conjugates†‡

Pau Moneva Lorente,[a] Antoine Wallabregue,[a] Francesco Zinna,[b] Céline Besnard,[c] Lorenzo Di Bari[b] and Jérôme Lacour*[a]

Received 1st September 2020,
Accepted 14th September 2020

DOI: 10.1039/d0ob01809k

rsc.li/obc

A series of chiral fluorescent helicene-BODIPY conjugates was prepared by the regioselective formylation of aza[4]helicene precursors and then an efficient one-pot two-step BODIPY synthesis (13 examples, 28–82%). Fused conjugates exhibit absorption and fluorescence properties (Φ_F 30–45%) in the red visible domain, and a CPL signature could be measured at 605 nm (g_{lum} ±5 × 10^{-4}). Photophysical and electronic properties were investigated and rationalized through first principles.

Introduction

Azahelicenes are *ortho*-fused polyaromatics that contain at least one sp^2 hybridized nitrogen atom embedded into the helical core. The presence of the heteroatom bestows these derivatives with added chemical reactivity and also electronic and (chir)optical properties that have been widely employed in asymmetric catalysis,[1–3] biochemistry,[4–7] solid-state self-assembly,[8–13] material sciences,[14–16] and chiral luminescence[15,17–26] Azahelicenes usually absorb in the UV spectral domain with low fluorescence efficiencies which are attributed to an intersystem crossing from singlet to triplet excited states (leading to deexcitation by phosphorescence or by non-radiative processes)[27] or to symmetry-forbidden $S_1 \rightarrow S_0$ transitions.[28] For the design of more effective azahelicene fluorophores, different synthetic strategies were considered,[29–31] including their fusion with boron-dipyrromethene dyes (BODIPYs).[31]

BODIPYs are generally characterized by their narrow absorption and emission bandwidths, covering the entire visible spectral range of light with high peak intensities, small Stokes shifts and high fluorescence quantum yields.[32–34] These properties arise from the tetracoordinated B(III) atom that conformationally locks the two nitrogen ligands. The induced stiffness and planarity of the whole dipyrromethene core allows a maximal extension of the conjugation.[35] Owing to their luminescence properties, BODIPYs have been actively explored over the last decades.[32,33,35] In the context of this study, asymmetric versions of such fluorophores have been reported in the literature,[29–31,36–43] *e.g.* **1–3** (Fig. 1), in which the chirality is brought by the presence of adjacent stereocenters, by the axial chirality of an allied BINOL ligand or even by the helical chirality of a fused helicene backbone. Herein, we report the synthesis and (chir)optical properties of a new family of chiral BODIPY derivatives **4** obtained by fusion with a cationic diaza [4]helicene scaffold; electronic, absorption and luminescence properties being rationalized using first principles.

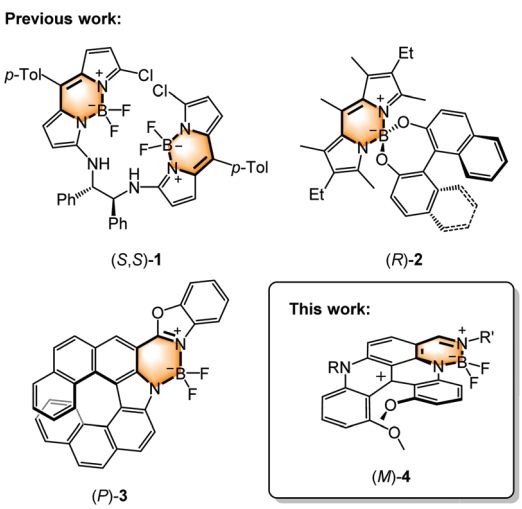

Fig. 1 Selected chiral BODIPYs. Configurations are shown arbitrarily.

[a]*Department of Organic Chemistry, University of Geneva, Quai Ernest Ansermet 30, 1211 Geneva 4, Switzerland. E-mail: jerome.lacour@unige.ch*
[b]*Università di Pisa, Dipartimento di Chimica e Chimica Industriale, Via G. Moruzzi 13, 56124 Pisa, Italy*
[c]*Laboratory of Crystallography, University of Geneva, Quai Ernest Ansermet 24, 1211 Geneva 4, Switzerland*

†The dataset for this article can be found at the following DOI: 10.26037/yareta:qs3vif5ggbc6jpanuricxbkrbm. It will be preserved for 10 years.

‡Electronic supplementary information (ESI) available: Experimental conditions, full characterizations, ^{1}H NMR, ^{13}C NMR, ^{19}F NMR and IR spectra of all new compounds; R_f and HRMS. CCDC 2024041. For ESI and crystallographic data in CIF or other electronic format see DOI: 10.1039/d0ob01809k

Results and discussion

Late-stage functionalization of quinacridinium salts

Previously, our group developed the two-step synthesis of NH-quinacridiniums of type **5** (Scheme 1).[44] These dyes are configurationally stable ($\Delta G^{\ddagger}$ = 30.7 ± 4.0 kcal mol^{-1} at 140 °C) and their enantiomers can be separated *via* chiral stationary phase (CSP) HPLC. Protonated and neutral conjugates display a perfectly reversible acid–base equilibrium (pK_a ~ 9.0) and their (chir)optical properties are modulated by the pH. For the quinacridinium salts, absorbance at low energy around 625 nm and emission around 690 nm with a fluorescence quantum yield of 0.6% and a lifetime of 0.45 ns in water were noted. As it was deemed important to improve the emission properties, fusion with a BODIPY skeleton was considered using a derivatization strategy and a late-stage functionalization approach. In fact, on chemically-related cationic helical DMQA$^+$ salts,[45,46] it was shown that these compounds are surprisingly electron-rich and behave as effective nucleophiles in S_EAr reactions. Consequently, NO_2 and CHO groups can be introduced regioselectively at the periphery of the helical scaffold.[23] With these results in mind, compounds **5** were subjected to Vilsmeier–Haack conditions and novel formylated derivatives **6** were obtained as single regioisomers (CHO introduced at position 6, Scheme 1). Alkyl-substituted **5a** (R = Pr) reacts more readily than **5b** (R = Ph); the formylation requiring only room temperature with **5a**. This is favorable to avoid bis- and tris-CHO functionalization and it simplifies purification. In terms of optical properties, both compounds **6a** and **6b** exhibit a hypsochromic shift compared to their precursors with absorption and emission maxima still in the orange-red domain (*e.g.* λ_{abs} 563 nm, λ_{em} 613 nm for **6b**, Fig. S1‡), as well as a notable increase in fluorescence quantum yields (Φ_F 39% for **6b**).

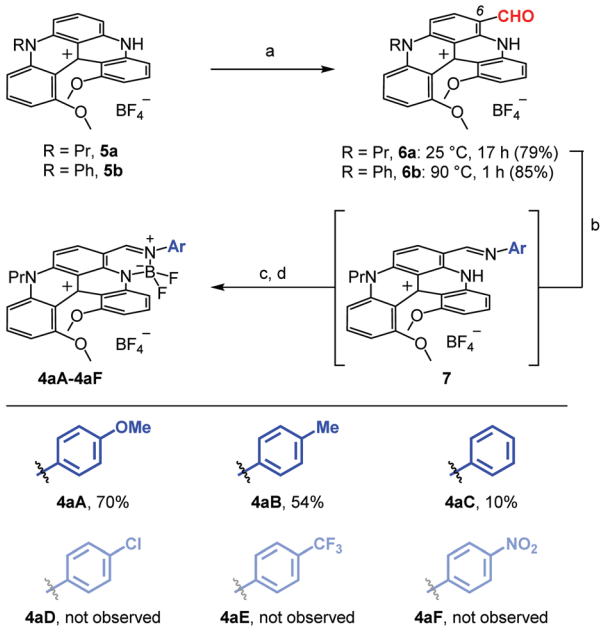

Scheme 1 Synthesis of fused helicene-BODIPYs **4** – Initial results. Reagents and conditions: (a) DMF (12 equiv.), $POCl_3$ (24 equiv.) and then H_2O 0–25 °C. (b) Ar–NH_2 (1.1 equiv.), CH_3CN, 60 °C, 1 h, MS (4 Å). (c) i-Pr_2NEt (5.5 equiv.), BF_3·OEt_2 (7.0 equiv.), CH_2Cl_2, 25 °C, 8 h. (d) $NaBF_4$ 0.2 M.

Initial results

With compound **6a** in hand, the formation of BODIPY analogues was started. A two-step one-pot protocol was considered *via* (i) a direct imine formation and then (ii) subsequent chelation with boron trifluoride. In a first set of experiments, six anilines were selected with various *para*-electron-donating and electron-withdrawing groups, EDGs and EWGs respectively. Standard conditions were selected involving a treatment of **6a** with 1.1 equivalents of $ArNH_2$ reagent in the presence of molecular sieves (4 Å). After 1 hour at 60 °C, the solvent was changed from acetonitrile to dichloromethane and the crude mixtures were immediately subjected to 5.5 equivalents of Hünig's base and 7.0 equivalents of BF_3·OEt_2. Mixed results were obtained as reactions with electron-rich anilines yielded the corresponding BODIPY derivatives (**4aA** 70%, **4aB** 54%) while low yield or no reactivity was obtained with aniline itself and derivatives substituted with EWGs (Scheme 1). For the latter problematic reactions, we could readily demonstrate that the first step of the protocol was the issue as only partial formation of the necessary imine intermediates **7** was observed in NMR spectroscopic analyses of crude reaction mixtures (data not shown).

Optimized two-step one-pot procedure

Modified conditions were thus looked to promote the imine formation with EWG-anilines. *p*-Nitroaniline **F** was selected for the screening study and the results are detailed in the ESI (Scheme S1‡). An optimal procedure was identified using the protocol reported by García Ruano and Cid with pyrrolidine as catalyst (10 mol%);[47] instantaneous formation of intermediate **7F** occurring now at room temperature. With these conditions in hand for the first step, the scope of the one-pot procedure could be extended and a series of fused helicene-BODIPYs was synthesized (Scheme 2). To a single exception, the two-step procedure is general and applicable for all types of amines, whether aryl, alkyl, or heterosubstituted. Compounds made from *para*-anilines were isolated in good to modest yields (**4aA** to **4aE**, 82–28%); the lowest being still obtained with EWGs due to the sensitivity of the products to chromatographic conditions which precluded the isolation of **4aF** specifically. Monocrystals of **4aE** were obtained and the crystallographic structure was determined by X-ray diffraction analysis (Fig. S9‡). *ortho*- and *meta*-OMe substituents did not lead to any reactivity difference and compounds **4aG** and **4aH** were isolated in good yields, 58% and 69% respectively. The protocol was then extended to BODIPY derivatives derived from alkylamines, compounds **4aI** to **4aM**. Their synthesis was achieved in good to modest yields (30–75%). In the case of **4aK** made from (*S*)-3,3-dimethylbutyl amine (ee 99.7%), 1 : 1 mixture of diastereoisomers was obtained which could not be separated by crystallization or chromatography. With

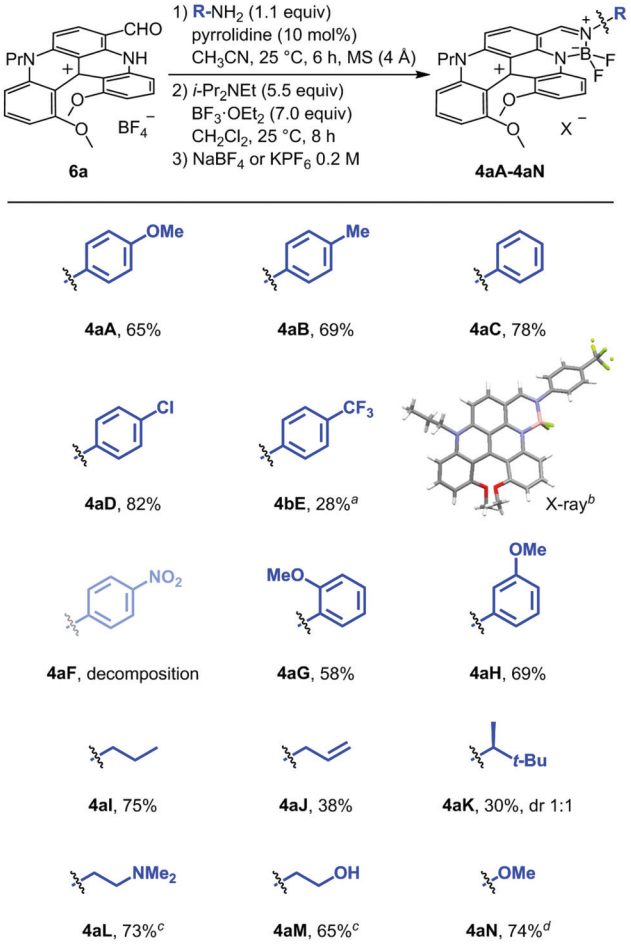

Scheme 2 Synthesis of **4aA** to **4aN** salts – optimized conditions. Unless otherwise noted, compounds **4** are isolated as tetrafluoroborate salts. [a] 2.2 equiv. of *p*-(trifluoromethyl)aniline were used. [b] Stick view of the crystal structure of **4aE** (BF_4^- omitted for clarity). [c] PF_6 salt. [d] 1.1 equivalents of $MeONH_2$·HCl + 1.1 equivalents of Et_3N.

aminoalkyl **L** and hydroxyalkyl **M** side chains, the corresponding products **4aL** and **4aM** displayed a strong increase in polarity and a counter-ion exchange from BF_4 to PF_6 anion was then necessary to improve their elution on silica gel. The ion metathesis was readily achieved after a wash with KPF_6 (0.2 M aqueous solution). Finally, synthesis of **4aN** made from NH_2OMe could also be achieved and the product was isolated in 74% yield.

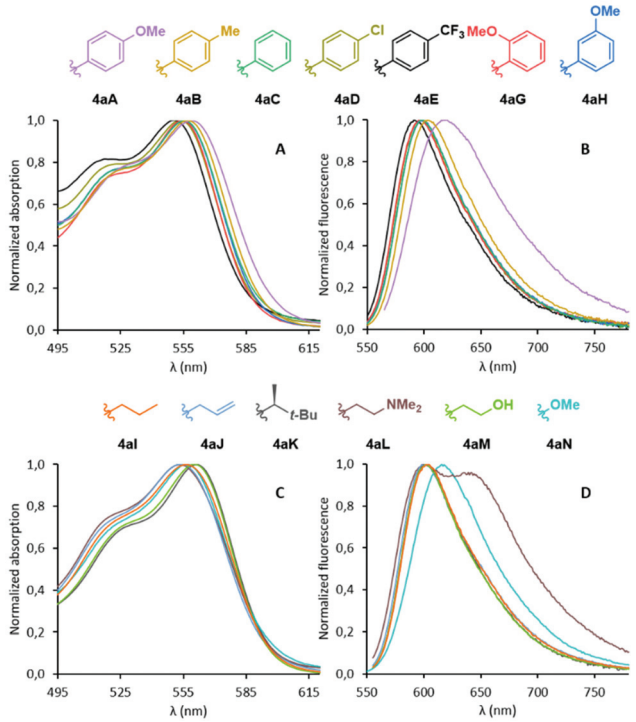

Fig. 2 Normalized absorption (A) and emission (B) spectra of compounds **4aA** to **4aH**. Normalized absorption (C) and emission (D) spectra of compounds **4aI** to **4aN**. Solutions in CH_3CN (10^{-5} M), λ_{exc} 560 nm.

Table 1 Photophysical properties of BODIPY derivatives **4**

Compound	λ_{abs} (nm)	ε_{max} (L mol^{-1} cm^{-1})	λ_{em} (nm)	Stokes shift (cm^{-1})	Φ_F [a] (%)
5[b]	625	12 700	690	1507	0.6
4aA	559	12 700	620	1760	4
4aB	557	16 300	603	1370	31
4aC	555	10 300	597	1268	32
4bC[c]	559	5600	598	1167	26
4aD	553	11 200	598	1361	31
4aE	550	10 900	591	1261	30
4aG	554	10 700	598	1328	24
4aH	555	9200	599	1324	36
4aI	556	13 900	604	1429	36
4aJ	554	13 200	601	1412	29
4aK	561	13 500	601	1186	41
4aL	553	11 600	602	1472	44
4aM	560	17 200	602	1246	46
4aN	556	10 600	616	1752	40

Solutions in CH_3CN (10^{-5} M). [a] Relative to cresyl violet (Φ_F = 54% in MeOH). Estimated error ±10%. [b] See ref. 35. [c] See Fig. S2.‡

(Chir)optical properties

With compounds **4aA** to **4aN** in hand, we turned our attention to their properties. Absorption and emission spectra were measured and the corresponding data is compiled in Fig. 2 and Table 1. In short, the optical properties are quite uniformed across the various derivatives. Differences are observed but the amplitude is modest ($\Delta\lambda_{abs}$ 11 nm and $\Delta\lambda_{em}$ 29 nm). In the case of aryl-substituted imines **4aA** to **4aH** (Fig. 2A and B), both absorption and fluorescence spectra showed a slight bathochromic shift in the presence of EDGs and, to the contrary, a small hypsochromic shift for EWGs. This behavior mimics the outcome of the functionalization of $DMQA^+$ at position 6 with EDGs and EWGs.[23] Compounds **4aB** to **4aH** present relatively strong quantum yields of fluorescence (24–36%, CH_3CN, 10^{-5} M) around λ_{em} 591–603 nm; only derivative **4aA** displaying a slightly red-shifted spectrum (λ_{em}

620 nm) and drastically lowered fluorescence efficiency (Φ_F 4%). This fluorescence quenching will be rationalized later based on first principles. With *N*-alkyl derivatives **4aI** to **4aN** (Fig. 2C and D), almost identical optical properties were also obtained, with slightly higher quantum yields than the aryl series, to the exception of **4aL** that displays a second transition at 639 nm in its fluorescence spectrum. This specific behavior is attributed to the formation of aggregates as a lowering of the concentration of **4aL** results in the fading of this band (Fig. S3‡). As a whole, absorption and emission values for compounds **4** exhibit a slight bathochromic shift compared to that reported by Maeda and Ema for their azahelicene-fused BODIPY analogues.[31]

For the study of the chiroptical properties, compound **4bC** was selected. Direct CSP-HPLC resolution of this adduct was not easily achievable and, hence, an enantiospecific synthesis starting from the single enantiomers (+)-(*P*)-**6b** and (−)-(*M*)-**6b** precursors was considered; the resolution of racemic **6b** being easier to achieve by CSP-HPLC than that of derivative **6a**.[44] Treatment of each enantiopure fraction with regular aniline and then $BF_3{\cdot}OEt_2$ afforded (+)-(*P*)-**4bC** and (−)-(*M*)-**4bC** in 80–88% yields. Electronic circular dichroism (ECD) spectra of the two samples displayed perfect mirror image from each other with three Cotton effects in the UV region (230, 275 and 345 nm) and only one transition in the visible domain (395 nm) (Fig. 3A). Like for $DMQA^+$ and other related [4]helicene derivatives, the $S_0 \rightarrow S_1$ transition centered around 560 nm does not have a strong chiroptical signature in ECD and we were not able to measure a reliable g_{abs} value for this transition.[23,48]

In circularly polarized luminescence (CPL), (+)-(*P*)-**4bC** and (−)-(*M*)-**4bC** displayed weak monosignate transitions with the maximum around 605 nm (Fig. 3B). The CPL spectra closely retrace the fluorescence spectrum (Fig. S5‡). The g_{lum} factor is about $\pm 5 \times 10^{-4}$ (see Fig. S4‡), in agreement with previously reported cationic diaza [4]helicenes.[17,23,24] However, these data highlighted a particularly intriguing result. Usually, for a single enantiomer, the sign of the CPL signal is identical to that of the lowest energy Cotton effect observed in ECD.[49] In the present case, the first measurable Cotton effect from the red-end of the spectrum falls at 395 nm and it is not associated with the $S_0 \rightarrow S_1$ transition.[50] Therefore, it cannot be compared to the $S_1 \rightarrow S_0$ transition observed in CPL.

Electrochemical properties

In addition, cyclic voltammetry (CV) analyses were performed *vs.* Fc/Fc^+ in anhydrous and degassed CH_3CN solutions containing $[Bu_4N^+][PF_6^-]$ (0.1 M) as supporting electrolyte. Some examples of cyclic voltammograms are presented in Fig. 4 and all redox potential data are summarized in Table 2. At first glance, we can observe that all derivatives of type **4** show analogous CV profiles, with two irreversible one-electron reductions around −1.15 and −1.45 V, and one irreversible one-electron oxidation around 1.25 V. Redox values are similar and little affected by the nature of the *N*-substituent, contrarily to $DMQA^+$ and its functionalized analogues.[23] In the aryl series, small variations are noticed nevertheless. E_1^{ox} values gently increase from **4aA** to **4aE** along with the electron-withdrawing ability of the substituents. Finally, two compounds behave differently with (i) *p*-MeO-phenyl-substituted derivative **4aA** exhibiting an extra irreversible one-electron oxidation at 1.34 V and (ii) Pr-substituted compound **4aI** presenting a different reduction profile (*pseudo*-reversible first and second negligible waves).

(TD)DFT calculations

To gain a better understanding of the spectroscopic and electrochemical properties of BODIPY derivatives **4**, DFT calcu-

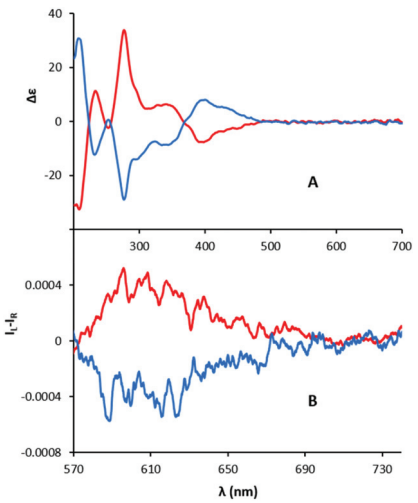

Fig. 3 ECD (A, *ca.* 10^{-5} M) and CPL (B, *ca.* 6.7×10^{-6} M) spectra of (+)-(*P*)-**4bC** (red line) and (−)-(*M*)-**4bC** (blue line). Solutions in CH_3CN. λ_{exc} 517 nm.

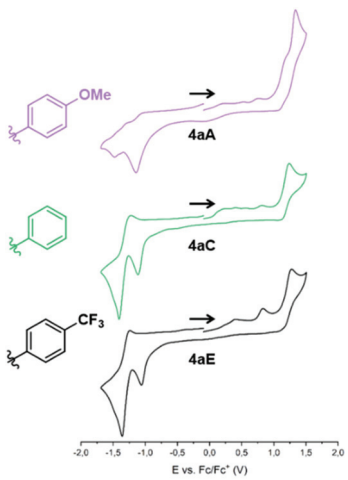

Fig. 4 Voltammetric curves of **4aA**, **4aC** and **4aE** (10^{-3} M) in acetonitrile ($[TBA][PF_6]$ 10^{-1} M) solutions recorded *vs.* Fc/Fc^+ at a Pt working electrode (⌀ = 3 mm, ν = 0.1 V s^{-1}).

Table 2 Cathodic and anodic potential values of derivatives **4a**

	Reduction		Oxidation	
Compound	E_1^{red} (V)	E_2^{red} (V)	E_1^{ox} (V)	E_2^{ox} (V)
4aA	−1.14	−1.48	1.19	1.34
4aB	−1.14	−1.48	1.23	—
4aC	−1.11	−1.41	1.24	—
4aD	−1.09	−1.46	1.26	—
4aE	−1.06	−1.36	1.28	—
4aG	−1.13	−1.41	1.24	—
4aH	−1.14	−1.49	1.24	—
4aI	−1.14[a]	—	1.20	—
4aJ	−1.16	−1.42	1.21	—
4aK	−1.20	−1.48	1.19	—
4aL	−1.20	−1.43	1.29	—
4aM	−1.18	−1.47	1.20	—
4aN	−1.11	−1.40	1.20	—

Values measured in CH_3CN (10^{-3} M), recorded experimentally *vs.* Fc/Fc^+ at a Pt working electrode (Ø = 3 mm, ν = 0.1 V s^{-1}) and containing [TBA][PF_6] as a supporting electrolyte (10^{-1} M). E_n^{red} and E_n^{ox} represent the n successive reduction and oxidation processes, respectively. Unless otherwise noted, all processes are irreversible. [a] *Pseudo*-reversible process.

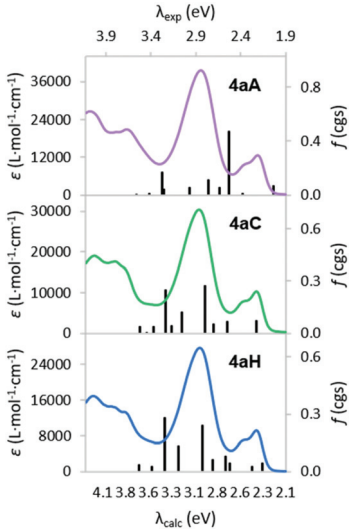

Fig. 5 Examples of computed excited states and experimental absorption spectra of BODIPY derivatives **4a**. 0.15 eV offset applied to all λ_{calc} axes. Computed at the B3LYP/6-311G(d,p) level of theory in gas phase.

lations were carried out using the Gaussian 09 software package.[51] The structure optimization of all compounds was carried out at the B3LYP[52]/6-311G(d,p) level of theory in gas phase. The analysis of the computed geometries highlights that all *para*-substituted aromatic rings in derivatives **4aA** to **4aE** show a 49° tilt angle with respect to the attached BODIPY framework, in agreement with the crystallographic data of **4aE**. *ortho*- and *meta*-Substituted aromatic rings in derivatives **4aG** and **4aH** display a slightly less pronounced inclination (*ca.* 45°).

To investigate the nature of the excited states involved in the absorption and emission bands, *ab initio* calculations were carried out (see ESI‡ for additional information). TD-DFT (Time Dependent Density Functional Theory) calculations were performed at the same level of theory and the first ten electronic vertical excitations were computed and compared to the experimental data (Fig. 5 and Table 3). It is known that hybrid functionals tend to provide accurate estimations with error ranges of 0.20–0.25 eV.[53] Consequently, B3LYP was chosen as the operating functional for this project. In order to make experimental λ_{abs} values concur with their $S_0 \rightarrow S_1$ transitions, a particularly low offset of 0.15 eV was needed. Range-separated hybrid functionals are also known to be particularly effective for charge-transfer electronically excited-states (EESs),[53] and CAM-B3LYP was then tested with derivative **4aC** as an example. Unfortunately, this functional proved a poorer precision (error = 0.70 eV) and it was hence discarded. Finally, calculations in acetonitrile as an implicit solvent were also carried out for derivatives **4aA** to **4aC**, but a slightly worse accuracy was obtained (error = 0.2 eV). Vertical excitation analysis indicates that the lowest energy band corresponds to HOMO → LUMO transition for most compounds, with the exception of **4aH** and **4aL** that present prevalent HOMO−1 → LUMO transition (see Fig. S7 and Tables S1–S17‡ for details).

Table 3 Experimental and computed transitions for compounds **4a**

		Calculated[a]		
Compound	Exp. λ_{abs} (eV)	λ_{abs} (eV)	f (cgs)	HOMO–LUMO gap (eV)
4aA	2.218	2.199	0.0695	2.60
4aB	2.226	2.364	0.0797	2.86
4aC	2.234	2.388	0.0711	2.91
4aD	2.242	2.381	0.0758	2.90
4aE	2.254	2.402	0.0666	2.94
4aG	2.238	2.344	0.0752	2.81
4aH	2.234	2.323	0.0427	2.71
		2.433	0.0283	2.98[b]
4aI	2.230	2.408	0.0589	2.95
4aJ	2.242	2.409	0.0591	2.95
4aK	2.210	2.408	0.0647	2.94
4aL	2.242	1.946	0.0059	2.29
		2.415	0.0649	2.85[b]
4aM	2.214	2.412	0.0559	2.96
4aN	2.230	2.388	0.0567	2.92

[a] Computed at the B3LYP/6-311G(d,p) level of theory in gas phase. [b] HOMO−1 → LUMO transition.

Not surprisingly, a discrepancy was observed for compound **4aA**, for which S0 → S1 transition is not fitting the experimental UV-Vis spectrum; the corresponding HOMO–LUMO gap being particularly low compared to the rest of the series (2.60 eV *vs.* 2.81–2.98 eV). As a consequence, frontier molecular orbitals (FMOs) responsible for the transition at the λ_{abs} were calculated of each compound of type **4** (Fig. S8‡). Their examination indicates that the nature of the *N*-substituent has an impact on the HOMO distribution, while the LUMO always remains unchanged. Aromatic-substituted derivatives increase the HOMO delocalization beyond the helical framework, the effect being more pronounced with EDGs than with EWGs (*cf.* Fig. 6). Also, the partial localization of the HOMO in the

p-MeO-phenyl substituent of derivative **4aA** suggests a possible photoinduced electron transfer (PET) process from this electron-rich aromatic group to the helical framework after UV light irradiation. This process would account for the observed fluorescence quenching of **4aA**. In support of this hypothesis, this effect can be seen, to a lesser extent, with derivative **4aG**. Conversely, non-aromatic substituents do not alter this distribution and the HOMO resides mainly in the helicene framework.

Rationale of the electronic properties

Computational studies were also performed to provide some insight into the electrochemical properties. As mentioned earlier, most derivatives **4** display two one-electron reductions and one one-electron oxidation processes; only compound **4aA** displaying an extra one-electron oxidation (Fig. S6‡ and Table 2). For this reason, with a wish to cover a maximum of redox processes, **4aA** was selected for the theoretical study. To locate the single unpaired electron after reduction or after oxidation, a calculation of the doublet spin state of **4aA** was thus carried out. The second set of calculations was performed for the doubly reduced and oxidized species respectively, and both singlet and triplet spin state energies were compared (Table 4). These analyses indicate that the first reduction takes place mostly at the central carbon 12 of the helicene (Fig. 7, left, blue dot). Regarding the second one-electron reduction, the energetic comparison within singlet and triplet spin states shows that the latter is slightly more stable (ΔE = 3.9 kcal mol^{-1}) and that a structure with two unpaired electrons is hence favored. In this case, the second unpaired electron is found at carbon 41 and, to a lesser extent, delocalized between carbons 5–11–26 (green dots). In the same manner, the oxidation processes also occur in two different regions, the first unpaired electron being delocalized between carbons 18–24–44 (Fig. 7, right, red dots) and the second one mostly at carbon 15 (orange dot).

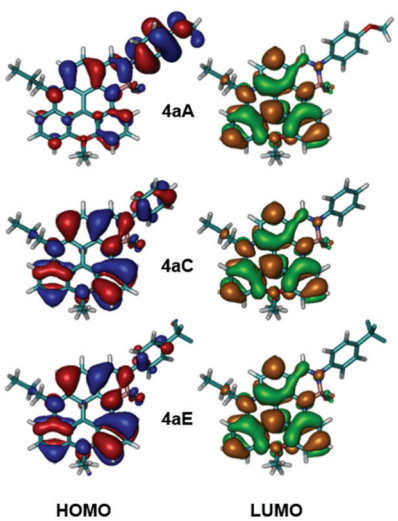

Fig. 6 Examples of HOMO (red and blue lobes) and LUMO (orange and green lobes) representations of compounds **4a** computed at the B3LYP/6-311G(d,p) level of theory in gas phase. Isovalues ±0.02.

Table 4 Redox processes: energetic values for compound **4aA**

Process	Charge	Multiplicity	Spin state	Energy (kcal mol^{-1})
1st red	0	2	Doublet	—
2nd red	−1	1	Singlet	0.0
	−1	3	Triplet	−3.9
1st ox	+2	2	Doublet	—
2nd ox	+3	1	Singlet	0.0
	+3	3	Triplet	−1.1

Computed at the B3LYP/6-311G(d,p) level of theory in gas phase.

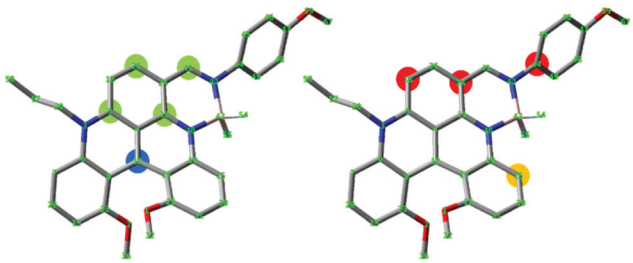

Fig. 7 Positions subjected to the 1st reduction (blue dot), 2nd reduction (green dots), 1st oxidation (red dots) and 2nd oxidation (orange dot) of BODIPY derivative **4aA**. Computed at the B3LYP/6-311G(d,p) level of theory in gas phase. Hydrogen atoms have been omitted for clarity.

Conclusions

Thanks to a late-stage Vilsmeier–Haack reaction, the regioselective formylation of diaza [4]helicenes **5** was achieved. Then, a one-pot two-step derivatization of **6** into fused helicene-BODIPY conjugates **4** was rendered possible by the use of pyrrolidine as a catalyst in the first imine formation step. The series of fluorophores were obtained in moderate to good yields (13 examples, 28–82%). These derivatives benefit from a strongly enhanced fluorescence compared to unfunctionalized precursors **5** and they display optical properties in the red visible domain. While an ECD signature could not be obtained at low energy, a CPL signal was nevertheless measured at 605 nm (g_{lum} ± 5 × 10^{-4}). The nature of the various substituents introduced on the BODIPY N-atom has, unfortunately, minor effects on their optical and electrochemical properties, as confirmed through first principles analyses.

Conflicts of interest

There are no conflicts to declare.

Acknowledgements

We thank the University of Geneva and the Swiss National Science Foundation for financial support (SNF 200020-172497 and 200020-184843). We acknowledge the contributions of the Sciences Mass Spectrometry (SMS) platform at the Faculty of Sciences, University of Geneva. We thank Dr Amalia I. Poblador-Bahamonde, Dr Johann Bosson and Dr Adiran de Aguirre for their advice concerning the computational experiments.

Notes and references

1 J. Chen and N. Takenaka, *Chem. – Eur. J.*, 2009, **15**, 7268–7276.
2 N. Takenaka, J. Chen, B. Captain, R. S. Sarangthem and A. Chandrakumar, *J. Am. Chem. Soc.*, 2010, **132**, 4536–4537.
3 P. Aillard, A. Voituriez and A. Marinetti, *Dalton Trans.*, 2014, **43**, 15263–15278.
4 R. Passeri, G. G. Aloisi, F. Elisei, L. Latterini, T. Caronna, F. Fontana and I. N. Sora, *Photochem. Photobiol. Sci.*, 2009, **8**, 1574–1582.
5 O. Kel, A. Fürstenberg, N. Mehanna, C. Nicolas, B. Laleu, M. Hammarson, B. Albinsson, J. Lacour and E. Vauthey, *Chem. – Eur. J.*, 2013, **19**, 7173–7180.
6 A. Babič, S. Pascal, R. Duwald, D. Moreau, J. Lacour and E. Allémann, *Adv. Funct. Mater.*, 2017, **27**, 1701839.
7 C. Bauer, R. Duwald, G. M. Labrador, S. Pascal, P. Moneva Lorente, J. Bosson, J. Lacour and J.-D. Rochaix, *Org. Biomol. Chem.*, 2018, **16**, 919–923.
8 E. Murguly, R. McDonald and N. R. Branda, *Org. Lett.*, 2000, **2**, 3169–3172.
9 C. Bazzini, T. Caronna, F. Fontana, P. Macchi, A. Mele, I. Natali Sora, W. Panzeri and A. Sironi, *New J. Chem.*, 2008, **32**, 1710–1717.
10 W. Shen, S. Graule, J. Crassous, C. Lescop, H. Gornitzka and R. Réau, *Chem. Commun.*, 2008, **7**, 850–852.
11 S. Graule, M. Rudolph, N. Vanthuyne, J. Autschbach, C. Roussel, J. Crassous and R. Réau, *J. Am. Chem. Soc.*, 2009, **131**, 3183–3185.
12 I. Alkorta, F. Blanco, J. Elguero and D. Schröder, *Tetrahedron: Asymmetry*, 2010, **21**, 962–968.
13 S. Graule, M. Rudolph, W. Shen, J. A. G. Williams, C. Lescop, J. Autschbach, J. Crassous and R. Réau, *Chem. – Eur. J.*, 2010, **16**, 5976–6005.
14 Y. Yang, R. C. da Costa, D.-M. Smilgies, A. J. Campbell and M. J. Fuchter, *Adv. Mater.*, 2013, **25**, 2624–2628.
15 J. R. Brandt, X. Wang, Y. Yang, A. J. Campbell and M. J. Fuchter, *J. Am. Chem. Soc.*, 2016, **138**, 9743–9746.
16 V. Kiran, S. P. Mathew, S. R. Cohen, I. Hernández Delgado, J. Lacour and R. Naaman, *Adv. Mater.*, 2016, **28**, 1957–1962.
17 J. E. Field, G. Muller, J. P. Riehl and D. Venkataraman, *J. Am. Chem. Soc.*, 2003, **125**, 11808–11809.
18 R. Hassey, E. J. Swain, N. I. Hammer, D. Venkataraman and M. D. Barnes, *Science*, 2006, **314**, 1437.
19 C. Shen, E. Anger, M. Srebro, N. Vanthuyne, K. K. Deol, T. D. Jefferson, G. Muller, J. A. G. Williams, L. Toupet, C. Roussel, J. Autschbach, R. Réau and J. Crassous, *Chem. Sci.*, 2014, **5**, 1915–1927.
20 N. Saleh, B. Moore II, M. Srebro, N. Vanthuyne, L. Toupet, J. A. G. Williams, C. Roussel, K. K. Deol, G. Muller, J. Autschbach and J. Crassous, *Chem. – Eur. J.*, 2015, **21**, 1673–1681.
21 N. Saleh, M. Srebro, T. Reynaldo, N. Vanthuyne, L. Toupet, V. Y. Chang, G. Muller, J. A. G. Williams, C. Roussel, J. Autschbach and J. Crassous, *Chem. Commun.*, 2015, **51**, 3754–3757.
22 J. Bosson, G. M. Labrador, S. Pascal, F.-A. Miannay, O. Yushchenko, H. Li, L. Bouffier, N. Sojic, R. C. Tovar, G. Muller, D. Jacquemin, A. D. Laurent, B. Le Guennic, E. Vauthey and J. Lacour, *Chem. – Eur. J.*, 2016, **22**, 18394–18403.
23 I. Hernández Delgado, S. Pascal, A. Wallabregue, R. Duwald, C. Besnard, L. Guénée, C. Nançoz, E. Vauthey, R. C. Tovar, J. L. Lunkley, G. Muller and J. Lacour, *Chem. Sci.*, 2016, **7**, 4685–4693.
24 S. Pascal, C. Besnard, F. Zinna, L. Di Bari, B. Le Guennic, D. Jacquemin and J. Lacour, *Org. Biomol. Chem.*, 2016, **14**, 4590–4594.
25 G. M. Upadhyay, H. R. Talele and A. V. Bedekar, *J. Org. Chem.*, 2016, **81**, 7751–7759.
26 J. R. Brandt, L. Pospíšil, L. Bednárová, R. C. da Costa, A. J. P. White, T. Mori, F. Teplý and M. J. Fuchter, *Chem. Commun.*, 2017, **53**, 9059–9062.
27 J. B. Birks, D. J. S. Birch, E. Cordemans and E. Vander Donckt, *Chem. Phys. Lett.*, 1976, **43**, 33–36.
28 H. Kubo, T. Hirose and K. Matsuda, *Org. Lett.*, 2017, **19**, 1776–1779.
29 E. M. Sánchez-Carnerero, F. Moreno, B. L. Maroto, A. R. Agarrabeitia, J. Bañuelos, T. Arbeloa, I. López-Arbeloa, M. J. Ortiz and S. d. l. Moya, *Chem. Commun.*, 2013, **49**, 11641–11643.
30 E. M. Sánchez-Carnerero, F. Moreno, B. L. Maroto, A. R. Agarrabeitia, M. J. Ortiz, B. G. Vo, G. Muller and S. d. l. Moya, *J. Am. Chem. Soc.*, 2014, **136**, 3346–3349.
31 C. Maeda, K. Nagahata, T. Shirakawa and T. Ema, *Angew. Chem.*, 2020, **59**, 7813–7817.
32 A. Loudet and K. Burgess, *Chem. Rev.*, 2007, **107**, 4891–4932.
33 N. Boens, V. Leen and W. Dehaen, *Chem. Soc. Rev.*, 2012, **41**, 1130–1172.
34 H. Lu, J. Mack, Y. Yang and Z. Shen, *Chem. Soc. Rev.*, 2014, **43**, 4778–4823.
35 D. Frath, J. Massue, G. Ulrich and R. Ziessel, *Angew. Chem., Int. Ed.*, 2014, **53**, 2290–2310.
36 Y. Wu, S. Wang, Z. Li, Z. Shen and H. Lu, *J. Mater. Chem. C*, 2016, **4**, 4668–4674.
37 H. Lu, J. Mack, T. Nyokong, N. Kobayashi and Z. Shen, *Coord. Chem. Rev.*, 2016, **318**, 1–15.

38 F. Zinna, T. Bruhn, C. A. Guido, J. Ahrens, M. Bröring, L. Di Bari and G. Pescitelli, *Chem. – Eur. J.*, 2016, **22**, 16089–16098.
39 M. Saikawa, T. Nakamura, J. Uchida, M. Yamamura and T. Nabeshima, *Chem. Commun.*, 2016, **52**, 10727–10730.
40 C. Ray, E. M. Sánchez-Carnerero, F. Moreno, B. L. Maroto, A. R. Agarrabeitia, M. J. Ortiz, Í. López-Arbeloa, J. Bañuelos, K. D. Cohovi, J. L. Lunkley, G. Muller and S. de la Moya, *Chem. – Eur. J.*, 2016, **22**, 8805–8808.
41 R. B. Alnoman, S. Rihn, D. C. O'Connor, F. A. Black, B. Costello, P. G. Waddell, W. Clegg, R. D. Peacock, W. Herrebout, J. G. Knight and M. J. Hall, *Chem. – Eur. J.*, 2016, **22**, 93–96.
42 R. Clarke, K. L. Ho, A. A. Alsimaree, O. J. Woodford, P. G. Waddell, J. Bogaerts, W. Herrebout, J. G. Knight, R. Pal, T. J. Penfold and M. J. Hall, *ChemPhotoChem*, 2017, **1**, 513–517.
43 J. Jiménez, L. Cerdán, F. Moreno, B. L. Maroto, I. García-Moreno, J. L. Lunkley, G. Muller and S. de la Moya, *J. Phys. Chem. C*, 2017, **121**, 5287–5292.
44 A. Wallabregue, P. Sherin, J. Guin, C. Besnard, E. Vauthey and J. Lacour, *Eur. J. Org. Chem.*, 2014, 6431–6438.
45 B. W. Laursen and F. C. Krebs, *Angew. Chem., Int. Ed.*, 2000, **39**, 3432–3434.
46 B. W. Laursen and F. C. Krebs, *Chem. – Eur. J.*, 2001, **7**, 1773–1783.
47 S. Morales, F. G. Guijarro, J. L. García Ruano and M. B. Cid, *J. Am. Chem. Soc.*, 2014, **136**, 1082–1089.
48 R. Duwald, J. Bosson, S. Pascal, S. Grass, F. Zinna, C. Besnard, L. Di Bari, D. Jacquemin and J. Lacour, *Chem. Sci.*, 2020, **11**, 1165–1169.
49 H. Tanaka, Y. Inoue and T. Mori, *ChemPhotoChem*, 2018, **2**, 386–402.
50 In most instances, the band around 400 nm is associated to the transition from HOMO−1 to LUMO+1.
51 M. J. Frisch, G. W. Trucks, H. B. Schlegel, G. E. Scuseria, M. A. Robb, J. R. Cheeseman, G. Scalmani, V. Barone, B. Mennucci, G. A. Petersson, H. Nakatsuji, M. Caricato, X. Li, H. P. Hratchian, A. F. Izmaylov, J. Bloino, G. Zheng, J. L. Sonnenberg, M. Hada, M. Ehara, K. Toyota, R. Fukuda, J. Hasegawa, M. Ishida, T. Nakajima, Y. Honda, O. Kitao, H. Nakai, T. Vreven, J. A. Montgomery Jr., J. E. Peralta, F. Ogliaro, M. J. Bearpark, J. Heyd, E. N. Brothers, K. N. Kudin, V. N. Staroverov, R. Kobayashi, J. Normand, K. Raghavachari, A. P. Rendell, J. C. Burant, S. S. Iyengar, J. Tomasi, M. Cossi, N. Rega, N. J. Millam, M. Klene, J. E. Knox, J. B. Cross, V. Bakken, C. Adamo, J. Jaramillo, R. Gomperts, R. E. Stratmann, O. Yazyev, A. J. Austin, R. Cammi, C. Pomelli, J. W. Ochterski, R. L. Martin, K. Morokuma, V. G. Zakrzewski, G. A. Voth, P. Salvador, J. J. Dannenberg, S. Dapprich, A. D. Daniels, Ö. Farkas, J. B. Foresman, J. V. Ortiz, J. Cioslowski and D. J. Fox, *Gaussian 09, Revision D.01*, Gaussian, Inc., Wallingford CT, 2009.
52 T. Yanai, D. P. Tew and N. C. Handy, *Chem. Phys. Lett.*, 2004, **393**, 51–57.
53 C. Adamo and D. Jacquemin, *Chem. Soc. Rev.*, 2013, **42**, 845–856.